Impact of inter-building longwave radiative exchanges on building energy performance and indoor overheating

Impact of inter-building longwave radiative exchanges on building energy performance and indoor overheating

Xiaoxiong Xie [a], Zhiwen Luo [a, *], Sue Grimmond [b], Ting Sun [b], William Morrison [b]

[a] School of the Built Environment, University of Reading, United Kingdom

[b] Department of Meteorology, University of Reading, United Kingdom

Word count of abstract: 191

Word count of text: 7215

*Corresponding author: Dr Zhiwen Luo; Email: z.luo@reading.ac.uk

Abstract

Despite inter-building longwave radiative exchanges playing an important role in determining building energy and environmental performance, simulation tools (e.g. EnergyPlus) simplify this by assuming the surface temperature of surrounding buildings to be equal to the air temperature, and therefore cause bias. Here we propose a 'spin-up' approach to update building external surface temperature using either air or the isolated building temperatures. Neighbourhoods with different plan area fraction of buildings (λ_P) are analysed to assess the impact on building external surface temperatures, cooling and heating energy demand as well as indoor overheating degree hours. Using the default EnergyPlus method causes a large bias in all metrics in a dense urban area (λ_P = 0.6) and climates assessed (cf. the new method): external wall temperature (3 °C less, midday median), annual energy demand for cooling (17.1% less) and heating (6.2% higher), annual overheating degree hours during the day (> 28 °C, 24.5% less) and night (> 26 °C, 60.1% less). These biases are larger at lower latitudes. Thus, neglecting the surroundings influence on inter-building longwave radiation impacts critical design considerations of building energy and thermal performance in dense urban

areas.

Keywords: Inter-building longwave radiation; Building energy simulation; Building surface temperature; Indoor overheating risk; Urban environment

Nomenclature

F View factor with subscripts (e.g. *boi→a*: boi to air)
subscripts
- *a* air
- *adj* adjacent
- *boi* building of interest
- *g* ground
- *sky* sky

T Temperature (K)
subscripts
- *a* Typical meteorological year (TMY) air temperature
- *adj* external surface of adj buildings
- *boi* external surface of boi
- *iso* external surface of isolated building
- *op* indoor operative (mean of air and radiant) temperature
- α albedo - external building facet
- λ_P plan area fraction

1. Introduction

The indoor thermal environment and cooling/heating energy consumption of buildings are affected by the local microclimate, including changes in longwave radiation from the surroundings. Longwave radiative exchange plays an important role in the urban heat island (Oleson et al., 2011), the urban energy balance (Oke, 1982), and in turn influences building energy performance (Santamouris et al., 2001). Ignoring longwave radiative exchanges with the surroundings in building energy simulations, can cause energy consumption to be overpredicted in winter and underpredicted in summer in mid-latitude cities (Bouyer et al., 2011).

Typically, building energy simulation (BES) tools are developed for isolated buildings and focus on the internal rather than external longwave radiation exchange (Allegrini et al., 2012; Evins et al., 2014) as obtaining both the external surface temperatures of the surroundings and the view factors in real urban areas is challenging (Yang et al., 2012; Evins et al., 2014).

BES longwave radiative exchanges between buildings are either pre-calculated using an urban climate model (e.g., TEB (Bueno et al., 2011), ENVI-met (Yang et al., 2012) and CitySim (Miller et al., 2018)), or indoor radiation schemes have been applied to surrounding external facets (so-called "false zone", e.g. Vallati et al. (2018) and Allegrini et al. (2016) in TRNSYS). Both approaches have been restricted to simple geometries (e.g. symmetric and low-rise street canyons) (Evins et al., 2014).

Commercial software (e.g. TRNSYS) by definition has more restricted availability than open-access software. Free, open-source BES tools (e.g. EnergyPlus) tend to be well evaluated and widely used to assess building energy performance (Chan, 2011; Liu et al., 2015; Ciancio et al., 2018; Yang et al., 2019) and overheating risks (Demanuele et al., 2012; Mavrogianni et al., 2012; Oikonomou et al., 2012; Virk et al., 2015; Hwang et al., 2017). Urban climate studies using EnergyPlus have addressed different sources of air temperature (e.g. Chan, 2011; Ciancio et al., 2018; Salvati et al., 2017; Yang et al., 2019), but very few consider longwave radiative exchanges from adjacent buildings (Evins et al., 2014; Luo et al., 2020).

Three approaches are used to address longwave radiative exchanges between buildings with EnergyPlus according to our mini-review (Table 1). By default (#1, Table 1), the surface temperature of both the ground and adjacent buildings are assumed to be equal to the air temperature from weather data input. However, typically, air temperature has a smaller range than surface temperatures. In practise, roofs have the largest range (Morrison et al., 2020, 2021) and walls are warmer during both the day and night (e.g. summer in London: south wall peak 15 °C warmer (cf. canopy air temperature peak), minimum 3 °C warmer (Morrison et al., 2020, 2021)). Also, the timing of the peak temperatures differs with air being later than facet surface temperatures apart from the east facet (e.g. peak air temperature around 4 hours later than the south wall peak surface temperature on a summer day in London (Morrison et

al., 2020, 2021)). Hence, using air rather than facet surface temperatures to derive longwave radiation is biased. This method assumes the view factors of the ground and adjacent buildings are equal to the residual of the sky (and further split into sky and air) view factors.

A second method (Evins et al. (2014), #2, Table 1) assigns surface temperatures of the building of interest (*boi*) to adjacent (*adj*)buildings. All buildings are assumed to have the same height. First, the *boi* wall temperatures are determined assuming it is isolated (*iso*). Second, these are assigned to the corresponding *adj* building (e.g., east-facing wall → east-facing wall). This neglects radiative exchanges for adjacent buildings.

In the third method (#3, Table 1), a new EnergyPlus sub-module allows view factors and *adj* facet surface temperatures to be supplied from an external source. Luo et al. (2020) assume the *adj* is isolated, therefore ignore the building density (i.e. plan area fraction) influence on surface temperature. They account for the real setting view factors by using Monte Carlo ray tracing. Although, the siting assumptions and view factors (e.g. values, methods) can be changed between applications, a more fundamental constraint is that the surface temperature data are a static time series that does not dynamically respond during the simulation.

Here, our aims are:

(1) to improve EnergyPlus' ability to account for longwave radiation from surrounding buildings impact on the external facets of a building of interest,

(2) to assess the impacts these model changes to simulated building surface temperature, building heating/cooling demand and indoor thermal environment (indoor overheating hours and degree-hours),

(3) to assess if these impacts are influenced by building density and/or climate,

(4) to assess if the impacts are sufficient to be regarded as an improvement to EnergyPlus simulation outcome.

Table 1: Methods used in EnergyPlus (E+) to calculate longwave radiation. View factor (F) are determined using ray-tracing with #3 using the Monte Carlos method (section 2.2 and SM.1). The temperatures of the ground (T_g) are assigned the Typical meteorological year (TMY) air temperature (T_a) in all three cases but the external surface of *adj* buildings (T_{adj}) are assigned different temperature between the three.

#	Urban geometry	View factors *(F)* considered	T_{adj}	Remarks	References
1	*boi* with *adj* buildings	$F_{boi→sky}$; $F_{boi→a}$ $F_{boi→g} + F_{boi→adj} = 1 - (F_{boi→sky} + F_{boi→a})$	T_a	default	Kesten et al. (2012), Oikonomou et al. (2012), Ramponi et al. (2014), Gracik et al. (2015), Han et al. (2017), Salvati et al. (2017), Vartholomaios (2017), Martinopoulos et al. (2018), Lima et al. (2019), Boccalatte et al. (2020)
2	Street canyon	$F_{boi→sky}$ and slope of the building surface $F_{boi→adj}$ for the street canyon	$T_{boi, iso}$	Needs: $F_{boi→adj}$, T_{adj}	Evins et al. (2014)
3	A real case	$F_{boi→adj}$ $1 - F_{boi→adj} = F_{boi→sky} + F_{boi→a} + F_{boi→g}$	$T_{adj, iso}$	Needs: $F_{boi→adj}$, T_{adj}	Luo et al. (2020)

2. Methods

To compare inter-building longwave radiative exchange using the available methods in EnergyPlus, the building of interest (*boi*) is simulated assuming either it is isolated (*iso*) or with adjacent (*adj*) buildings at different densities and climates. To undertake this work, we use an idealised neighbourhood (3 × 3 aligned single-zone buildings). EnergyPlus Version 9.4 (U.S. Department of Energy, 2020a) is used.

2.1.Building energy simulation setup in EnergyPlus

In this study we use the reference building BESTEST Case 600 from ANSI/ASHRAE Standard 140-2011 (ANSI/ASHRAE, 2011) for the analyses. This lightweight construction building (thermal properties are summarized in Table 2) is 8 m wide x 6 m long x 2.7 m tall, with no interior partitions, and two 2 m x 3 m windows on the south-facing wall. An ideal load system is assumed with a winter heating setpoint of 20 °C and summer cooling setpoint of 27 °C. The ventilation rate is 0.5 air change per hour (ACH). The internal heat load is constant at 200 W and assumed to be 100% sensible heat. To compare indoor overheating risks, the free-running building BESTEST Case 600 FF is used. Unlike Case 600, there is no mechanical heating or cooling system but everything else is the same (e.g. ventilation rate

remains 0.5 ACH).

When the *boi* has adjacent buildings, they are all identical (Fig. 1). Given its replicability and generalisability, this idealised building has been widely used in neighbourhood-scale building energy simulation studies (e.g. #1, Table 1) (Liu et al., 2015). Building densities, characterised by the plan area fraction (λ_P), are varied (0.1, 0.3, 0.6) to cover a range found in real cities (Grimmond and Oke, 1999). The *adj* buildings modify the radiative exchanges. View factors (F) between the *boi* surfaces and *adj* surfaces are calculated with Monte Carlo ray-tracing method (Howell et al., 2010) (Section 2.2). TMY (typical meteorological year) data (ASHRAE, 2001) for three cities with similar longitude but different latitudes are chosen, hence different daylengths and climates are investigated: London (51.15° N, 0.18° W), Aberdeen (57.20° N, 2.22° W) and Marseille (43.45° N, 5.23° E). The 10-min timestep simulations are used to assess convergence of the surface temperature but hourly sample are analysed.

Table 2: Main features of construction elements from ANSI/ASHRAE (2011), with the normal incidence window albedo given modified by incident angle (Arasteh et al., 2009).

Element	Materials	U-value	α	ε
Walls	Plasterboard, fiberglass quilt, wood siding	0.514	0.4	0.9
Roof	Plasterboard, fiberglass quilt, roof deck	0.318	0.4	0.9
Floor	Timber flooring, insulation	0.039	0.4	0.9
Windows	Double-pane glass	3.0	0.078	0.9

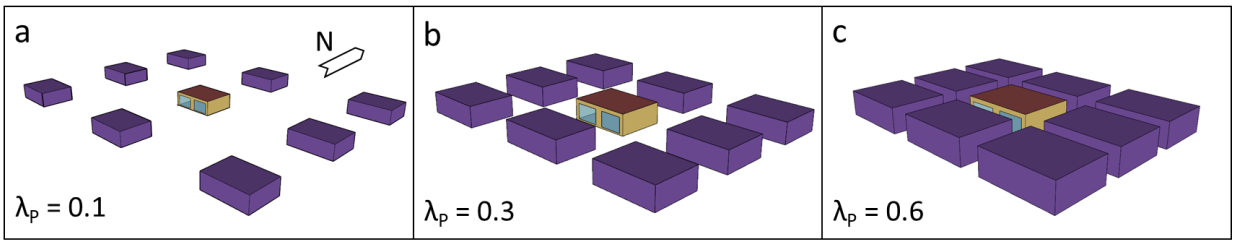

Fig. 1. Building of interest (*boi*) is in the centre of eight adjacent buildings (*adj*, purple), with different plan area fractions (λ_P): (a) 0.1, (b) 0.3, and (c) 0.6.

2.2.Inter-building longwave radiation exchange

The longwave radiative exchange between surfaces depends on surface temperature, spatial relations between surfaces and surroundings, and material properties of the surfaces (U.S.

Department of Energy, 2020b). In the absence of more detailed information, the EnergyPlus default setting assumes (U.S. Department of Energy, 2020b): the ground is flat; the external surface temperature is equal to air temperature in the weather data input; all surfaces (including the ground) are opaque grey bodies; have isotropic emissivity; have uniform surface temperatures; no longwave reflection occurs; and across a sphere the total view factor (=1) from a building surface consists of only sky, ground, and buildings (U.S. Department of Energy, 2020b).

Previously, EnergyPlus obtains surface temperature data for an adjacent building (T_{adj}) from (Fig. 2): (1) TMY air temperature (T_a) (#1, Table 1), or (2) calculated surface temperatures for an isolated building (T_{iso}) (#2,3, Table 1). However, neither represents conditions where *adj* buildings are also influenced by other buildings in the neighbourhood. In this study, we determine the *adj* surface temperature using the Luo et al. (2020) sub-module. However, as Luo et al. (2020) originally used static surface temperatures, we investigate the impact of building surface temperatures used on model spin-up on the results as this is important in urban areas (Best and Grimmond, 2014). Luo et al. (2020) uses static surface temperature time series which does not update after each iteration. In our new method, we spin-up the model by updating the building surface temperature from the previous run, until the EnergyPlus convergence criteria are met. Since EnergyPlus cannot calculate the external ground surface temperatures, they remain equal to TMY air temperatures (i.e. the default setting in EnergyPlus).

For example, if the building of interest (*boi*) surface temperatures are obtained from an *adj* building that is isolated (T_{iso}) after *i* iterations (indicated as $boi_{adj \leftarrow iso,i}$), this involves the following steps (Fig. 2): (1) EnergyPlus is run for the entire year to obtain boi_{iso} (isolated *building of interest*) surface temperature T_{iso} at each time step; (2) T_{iso} is assigned to the *adj*

buildings to initialise them by facet (e.g. surface temperature of N wall of boi_{iso} is assigned onto the N wall of *adj* buildings as a yearlong EnergyPlus schedule file in csv format, and so as for other three facets.) All buildings are identical; (3) EnergyPlus is re-run to obtain the surface temperatures of $boi_{adj\leftarrow iso}$ for the year; (4) Repeat Step (2), surface temperatures of $boi_{adj\leftarrow iso}$ are assigned to $boi_{adj\leftarrow iso,1}$ as T_{adj}; and, (5) so on for each *i* with convergence assessment made for each wall facet. For external surface temperatures of each facet, this convergence criteria is 0.01 °C (Winkelmann, 2001). Iteration stops when the annual mean bias error (MBE, Section 2.4) between the current and previous iteration of each facet is within ±0.01 °C. Similar procedures are applied for $boi_{adj\leftarrow a,i}$ with T_a used for initialisation.

In these simulation, although other variables (e.g. air temperature, wind) that are also impacted by the surroundings (Tang et al., 2021), they do not vary from their original TMY values at each time step.

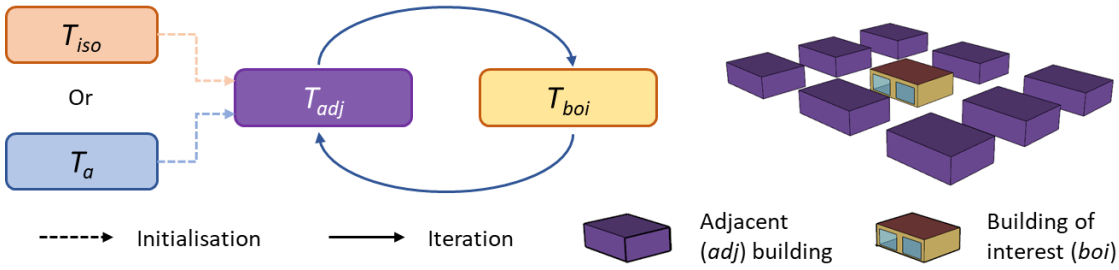

$boi_{adj\leftarrow iso}$	T_{adj} from T_{iso}	$boi_{adj\leftarrow iso,i}$	i^{th} iteration after $boi_{adj\leftarrow iso}$
$boi_{adj\leftarrow a}$	T_{adj} from T_a	$boi_{adj\leftarrow a,i}$	i^{th} iteration after $boi_{adj\leftarrow a}$

Fig. 2. Simulation workflow for different cases with T_{iso} or T_a used as the initial T_{adj}. In subsequent iteration T_{adj} is used to calculate T_{boi}, and T_{boi} used for T_{adj} in the next simulation.

If T_a is assigned to *adj* buildings ($boi_{adj\leftarrow a}$), the default EnergyPlus view factor calculation method is used. As ground and *adj* buildings are assumed to have the thermal characteristics of air (U.S. Department of Energy, 2020b), the *boi* surface to non-sky surfaces view factor is obtained by subtracting the sky view factor from 1. It is assumed that the sky longwave

radiance distribution is isotropic.

When surrounding buildings exist, EnergyPlus calculates the sky view factor for 144 points (6 zeniths x 24 azimuths) evenly distributed across the sky dome. The view factor is the fraction of building external surfaces receiving points (4 points per facet, the rectangular area is defined by its length and width) relative to the 144 sky dome points (U.S. Department of Energy, 2020c).

For the $boi_{adj \leftarrow iso}$ we follow Luo et al. (2020) and use a Monte Carlo ray-tracing approach from the building surface (Howell et al., 2010):

$$F_{1\rightarrow 2} = \frac{A_2}{n}\sum_{i=1}^{n}\frac{\cos\theta_1 \cos\theta_2}{\pi r^2} H_{block} \qquad (1)$$

where n is the number of pairs of randomly points on surfaces 1 and 2, A_2 the area of surface 2, r the ray length, θ is the angle between the ray and the surface normal, H_{block} indicates if the ray is blocked by other surfaces (= 0, obstructed) or not (= 1). In this study, we find n = 3000 to be sufficient by comparing the Monte Carlo method to analytical results (section SM. 1).

With view factors to *adj* building surfaces determined, the sky and ground view factors are given by the residual ($1 - \sum F_{adj}$). As all buildings in the neighbourhood are the same size, $F_{boi \rightarrow g}$ and $F_{boi \rightarrow sky}$ are equal. To reduce computational cost, we assume each *adj* building facet has uniform surface temperatures independent of material variations (e.g. glass, concrete) (Evins et al., 2014; Luo et al., 2020). Impact of this simplification has been analysed and the surface temperature difference is suggested to be smaller than 0.2 °C (section SM. 2).

2.3. Building heating/cooling load and overheating risk

Heating and cooling loads are calculated for Ideal Loads Air System with 100% efficiency (U.S. Department of Energy, 2020d) and setpoints of 20 °C for heating in winter and 27 °C

for cooling in summer. The indoor overheating risk within free-running buildings is assessed based on the degree hours (Zhang et al., 2006; Porritt et al., 2011, 2012) exceeding indoor operative temperature thresholds of CIBSE Guide A (CIBSE, 2006) (28 °C for the living area and 26 °C for the bedroom). Given the single-zone *boi*, we split the day based on occupancy into night ('bedroom', 23:00 to 7:00) and day ('living room', 07:00-23:00) (Porritt et al., 2012). The CIBSE overheating thresholds, determined for the UK climate, may not be directly applicable to other climates, however, we use them in all climates (i.e. including Marseilles) for consistency in the comparisons.

2.4. Analysis metrics

Mean absolute error (MAE) and mean bias error (MBE) are used to assess the difference in surface temperatures between iterations:

$$MAE = \frac{1}{N}\sum_{j=1}^{N}\left|y_j - x_j\right| \qquad (2)$$

$$MBE = \frac{1}{N}\sum_{j=1}^{N}\left(y_j - x_j\right) \qquad (3)$$

where y_j and x_j are data from two cases at instance j, and N is the number of values analysed (e.g. a year with 10-min timestep, N = 52560). The distribution of hourly surface temperature variances between iterations is analysed in Section 3.1.

The normalised mean bias error is used in multiple guidelines for uncertainty analysis of building energy simulation programmes (Ruiz and Bandera, 2017):

$$nMBE = \frac{1}{N}\frac{\sum_{j=1}^{N}\left(y_j - x_j\right)}{\bar{x}_j} \times 100\% \qquad (4)$$

In this study, we use nMBE to compare the hourly load variance between different cases. The ASHRAE Guideline 14 (ASHRAE, 2014) sets the uncertainty limits for building energy simulation programmes as nMBE within ±10% for hourly data.

For annual energy demand and overheating degree hour comparisons, the percentage difference is calculated as the ratio of difference between cases to the base case.

2.5.Evaluation of longwave radiative exchange with observations

To evaluate the longwave radiative calculations, surface temperature observations (Morrison et al., 2021, 2018) conducted at the Comprehensive Outdoor Scale Model (COSMO) test site (Kanda et al., 2007) are used. The 100 m × 50 m site has 32 × 16 aligned arrays of 1.5 m cubic concrete blocks (0.1 m wall thickness, λ_P = 0.25). The long axis is oriented 49° west of true north.

Surface brightness temperatures were measured with two Optris PI160 LWIR cameras (Optris GmbH, Germany) facing north (Fig. 3a) and south. The measurements for a predominantly clear-sky day (2nd August 2014) are selected for evaluation. The experimental setup is reproduced in EnergyPlus consisting of 3 × 3 array of concrete cubes all with the same size and thickness (0.1 m dense concrete wall, conductivity = 1.63 W m^{-1}K^{-1}, density = 2300 kg m^{-3}, specific heat = 1000 J kg^{-1}K^{-1} (CIBSE, 2006)). EnergyPlus simulations of brightness temperatures are compared to the observations (Fig. 3b,c) by treating the concrete blocks as blackbodies (i.e. by assuming emissivity = 1 in EnergyPlus simulations). The weather data used in the EnergyPlus simulations are measured at the site or nearby (Morrison et al., 2021, 2018).

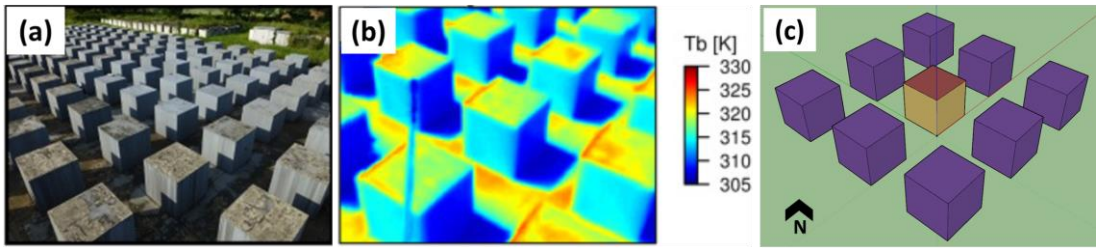

Fig. 3. Comprehensive Outdoor Scale Model (COSMO) test site in Japan (a) view near the north-viewing longwave infrared camera location, (b) brightness temperature (T_b) from the north-viewing camera at 2nd August 2014 10:00 local standard time, (c) model geometry used in EnergyPlus. Sources (a,b): Morrison et al. (2018).

3. Results

3.1.Impact of iteration on surface temperature

First, we assess if using an iterative approach (model spin up) to obtain external building surface temperature of surrounding buildings could impact the model surface temperature (Fig. 4). In all test cases, the mean bias error (MBE) indicates that there is a difference in surface temperature (i.e. MBE is not 0 °C) between the first and second iteration.

As neighbourhood density impacts both the shortwave and longwave radiative exchanges; for example, shadows and receipt of longwave radiation are very different with adjacent buildings (cf. isolated building), we assess if the impact of interactions varies with plan area fraction (λ_P). The number of iterations needed to meet the surface temperature convergence criteria (<0.01 °C) increases with urban density. At the lowest building density considered (λ_P = 0.1, Fig. 1) only two iterations are needed, increasing to three for λ_P = 0.3, and five when λ_P = 0.6 (Fig. 4). This is expected as the building of interest (*boi)* becomes increasingly influenced by the surroundings. At λ_P = 0.6, both the south-facing and north-facing walls of $boi_{adj \leftarrow iso,i}$ require more iterations to converge than other facets as they have largest difference between the initial and final surface temperatures. In addition to MBE, the distribution of surface temperature differences between $boi_{adj \leftarrow a,4}$ and $boi_{adj \leftarrow a,5}$ at λ_P = 0.6 are shown in Fig. 5. For the north-facing wall with the largest difference, there are 93.6% of time steps within the convergence criteria of ±0.01°C, while for other facets the fraction is higher than 99%.

Second, we consider the impact of source of the initial surface temperatures values (i.e. $boi_{adj \leftarrow iso.i}$ and $boi_{adj \leftarrow a.i}$). The difference between the two sources is large for the first iteration, up to 1.15 °C in the dense neighbourhood (λ_P = 0.6), but negligible in the low-density neighbourhood (λ_P = 0.1). Obviously, with each iteration their difference decreases (Fig. 4, 6) indicating that by updating T_{adj} it can modify an initial common value independent

of the initial surface temperature chosen. As $boi_{adj \leftarrow iso,5}$ and $boi_{adj \leftarrow a,5}$ have very similar surface temperatures, hereafter three representative cases are analysed:

(i) $boi_{adj \leftarrow a}$ using the default EnergyPlus method ('base');

(ii) $boi_{adj \leftarrow iso}$ following Luo et al. (2020) (no iteration); and

(iii) $boi_{adj \leftarrow a,5}$ the most realistic case with initialisation from TMY air temperature and five iterations.

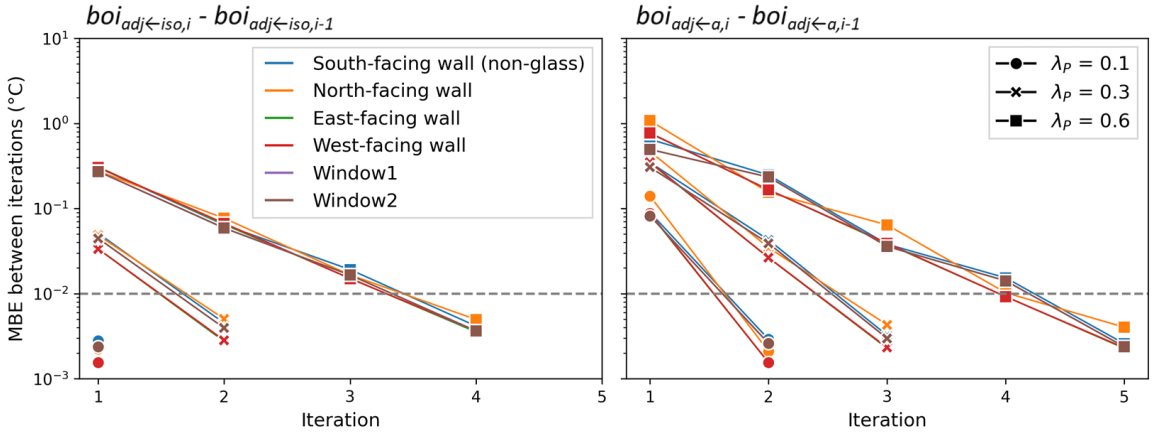

Fig. 4. Annual mean bias error (MBE, section 2.4; 10-min timestep, N=52560) determined using the external building surface temperature of the previous iteration (Fig. 2) for different facets (colour) in London with three plan area fractions (λ_P) (marker) and two initial *adj* surface temperatures (columns) with convergence criteria (0.01 °C, dashed line). Seasonal MBE and annual MAE are shown in section SM.3.

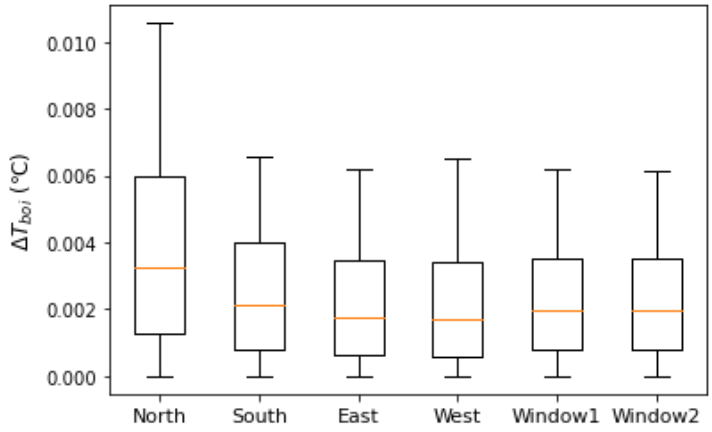

Fig. 5. Distribution of facet surface temperature differences (10-min timestep, N=52560) between $boi_{adj \leftarrow a,5}$ and $boi_{adj \leftarrow a,4}$ at λ_P = 0.6 with interquartile range (box), median (horizontal line) and 5th and 95th percentiles (whiskers).

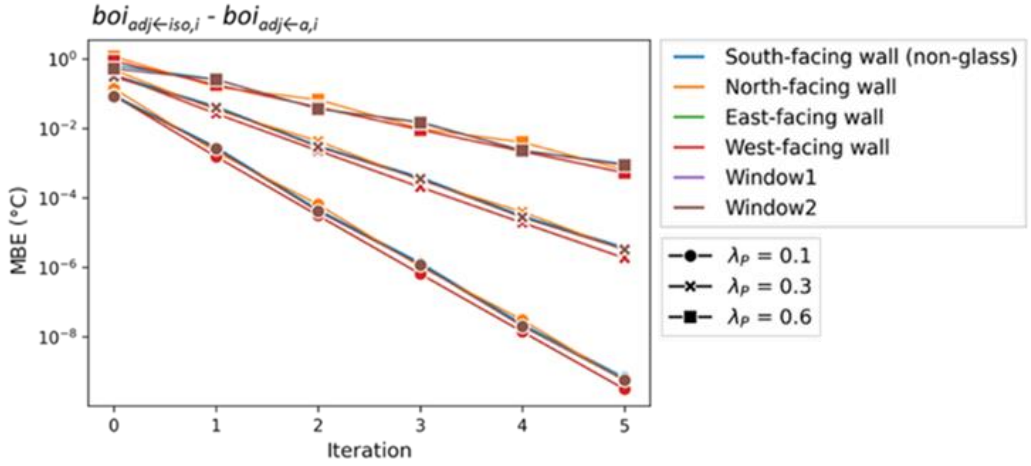

Fig. 6. As Fig. 4, but with different initial surface temperatures for different facets (colour) and plan area fractions (λ_P) (marker). Iteration 0 is $boi_{adj\leftarrow iso} \rightarrow boi_{adj\leftarrow a}$. Seasonal MBE and annual MAE are shown in Section SM.4.

3.2.Evaluation of simulated brightness temperatures with observations

The EnergyPlus simulated brightness surface temperatures using the above three methods can capture the main trend of observed diurnal pattern in an urban context (λ_P = 0.25, Fig. 3) (Fig. 7). The proposed improvement ($boi_{adj\leftarrow a.5}$) results are more similar to the observations than the default method ($boi_{adj\leftarrow a}$). $boi_{adj\leftarrow a,5}$ brightness temperatures are slightly larger (0.1 °C in average) than $boi_{adj\leftarrow iso}$ in this area because of the relatively low λ_P. It is expected that such difference will be much obvious when λ_P is high. This will be discussed in section 3.3.

The simulated surface temperatures are impacted by the ground surface temperature being set to the same as air temperature, whereas it will have a larger range: warmer during the day and depending on view factors cooler/warmer at night (e.g. summer in London: impervious ground peak 10 °C warmer (cf. canopy air temperature peak), minimum 3 °C warmer (Morrison et al., 2020)). Therefore, assigning the air temperature to the ground can potentially underpredict the longwave radiation received by building external walls, and hence underpredict the wall surface temperatures.

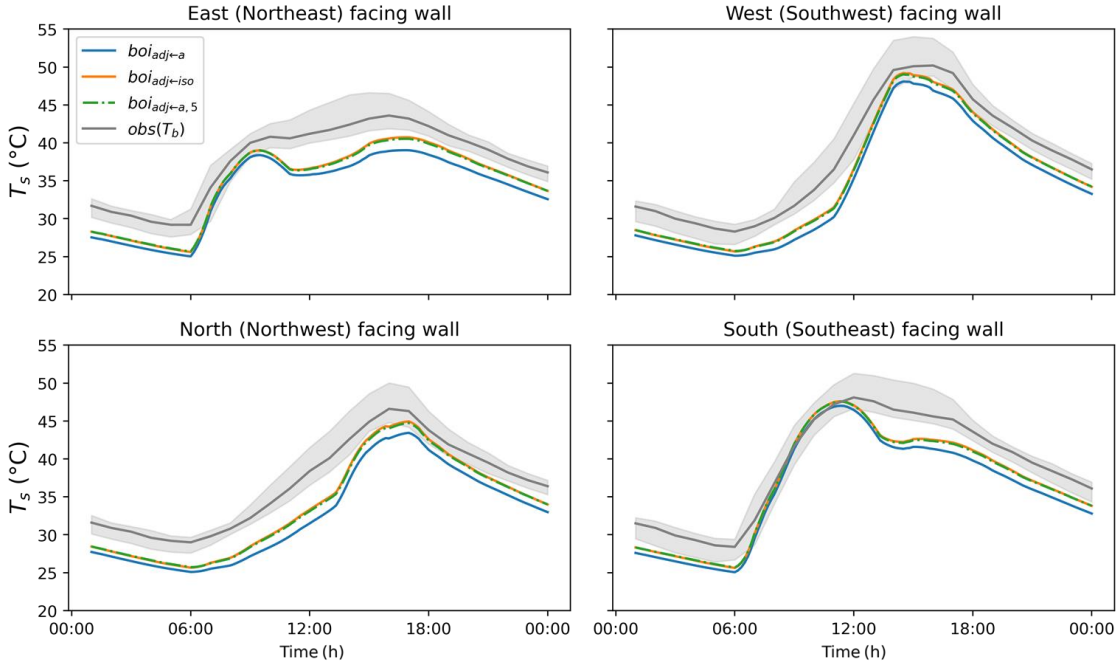

Fig. 7. Comparison of simulated (assuming emissivity = 1, 10-min) and observed (hourly median, line) brightness temperatures (5th and 95th percentiles: shading) at the COSMO site (Fig. 3) on 2nd August 2014. Observations are data from Morrison et al.'s Fig. 10c (2018).

3.3.External wall (opaque part) surface temperature in London

The longwave radiative calculation method selected (Section 3.1) changes the external building surface temperature diurnal cycle by facet orientation (Fig. 8a-f: north facing wall, g-x: south-facing wall - non-glass part). As expected, peak differences occur near solar noon, and when external surface temperatures are warmer than air temperature (Morrison et al., 2020, 2021).

The neighbourhood density impacts the *boi* external building surface temperatures. The smallest differences between methods occurs for the lowest-density (λ_P = 0.1) neighbourhood. These differences are smaller at night (0.8 °C) than during the day (3 °C) in summer (Fig. 8c), and varies less in the winter (night=1 °C; day=1.5 °C, Fig 8f) for the north-facing wall. The south-facing wall surface temperature differences are smaller, but the median difference at midday is still as large as 2 °C in summer (Fig. 8i) and 1.2 °C in winter (Fig. 8l). This suggests the default method ($boi_{adj\leftarrow a}$, #1, Table 1) in EnergyPlus introduces biases to the surface temperature in dense urban areas at London's latitude. As the external

345 building surface temperature is an important variable in EnergyPlus-related coupling (Zhang
346 et al., 2013), such biases can result in further uncertainties.

347 The diurnal temporal pattern differs among the three methods, for example, timing of the
348 surface temperature peak. In winter the north-facing wall (λ_P = 0.6) surface temperature
349 assigned from isolated building to *adj* buildings ($boi_{adj \leftarrow iso;}$ cf. $boi_{adj \leftarrow a}$) peaks later than the
350 one after five iterations using the air temperature initially ($boi_{adj \leftarrow a,5}$; cf. $boi_{adj \leftarrow a}$) (Fig. 8f).
351 The south-facing wall of the *iso* building is heated by the sun, surface temperatures continue
352 to increase for a longer period after noon, and leads to more longwave radiation exchange for
353 the *boi* north-facing wall. While for $boi_{adj \leftarrow a,5}$, south-facing wall of the *adj* building becomes
354 shaded around noon, so the longwave radiation starts to decrease earlier than for $boi_{adj \leftarrow iso}$.

355 Daytime in winter, the north-facing wall surface temperature difference between $boi_{adj \leftarrow iso}$
356 and $boi_{adj \leftarrow a}$ is higher than for the other facet orientations for the denser areas (λ_P = 0.3 and
357 0.6; Fig. 8e, f). With the lower solar altitude in winter, much less direct solar radiation is
358 received by the south-facing wall in denser neighbourhoods. Thus, the difference in south-
359 facing wall (non-glass area) surface temperature between shaded and isolated buildings
360 becomes much larger and further influences the longwave radiation calculated. This
361 difference is more evident on days with larger fluxes (e.g. 75th percentile) than the median
362 (Fig. 8f), because of the high frequency of winter cloudy periods (in the London TMY data)
363 which reduces the solar radiation differences between isolated and surrounding buildings.
364 Whereas on a clear winter day (30th December, i.e. at the 75th percentile), a large diurnal
365 cycle of $boi_{adj \leftarrow iso}$ occurs (Fig. 9). During the midday hours, the $boi_{adj \leftarrow iso}$ surface temperature
366 is greater than $boi_{adj \leftarrow a,5}$ by 2 °C. This does not occur for the south-facing wall, as the
367 opposite *adj* north-facing walls are less influenced by the solar radiation compared to *adj*
368 south-facing wall.

The night-time surface temperature from the $boi_{adj\leftarrow iso}$ method is cooler overall than when the $boi_{adj\leftarrow a,5}$ method is used, because of the lack of nocturnal longwave trapping. The underprediction is largest when λ_P = 0.6. These surface temperature differences are up to 0.6 °C.

View factors calculated by the EnergyPlus default method (i.e. as in $boi_{adj\leftarrow a}$) and Monte Carlo ray-tracing method (i.e. used in the following iterations) may introduce uncertainties. To address such impact, similar comparisons (as Fig. 8) are made in Fig. 10 but with surface temperatures of $boi_{adj\leftarrow a}$ simulated with the updated method (input T_{adj} and view factors independently). Results suggest that comparing with the updated view factor calculating method for $boi_{adj\leftarrow a}$, the default method by EnergyPlus tends to underpredict surface temperatures of $boi_{adj\leftarrow a}$. Such underpredictions are greater at λ_P = 0.3 and 0.6, which are up to 0.3 °C and 0.5 °C in median, respectively. The increase in surface temperatures of $boi_{adj\leftarrow a}$ hence reduces difference between it and the other two cases ($boi_{adj\leftarrow iso}$ and $boi_{adj\leftarrow a,5}$), especially at night due to the relatively smaller differences, but variations between spin-up ($boi_{adj\leftarrow a,5}$) and non-spin-up ($boi_{adj\leftarrow iso}$ and $boi_{adj\leftarrow a}$) methods still exist.

In summary, the $boi_{adj\leftarrow iso}$ method causes large differences in wall surface temperatures compared to the method with the most iterations/spin-ups ($boi_{adj\leftarrow a,5}$). These differences are most evident at night and in the winter near noon.

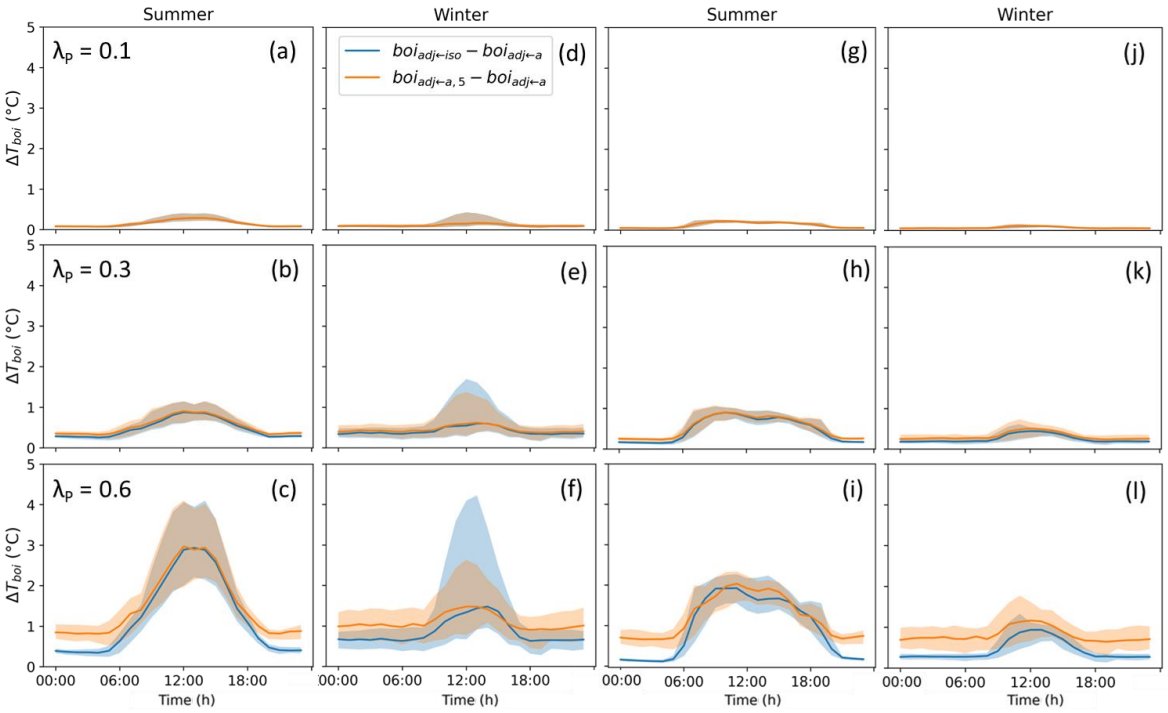

Fig. 8. Median diurnal cycle (lines) and inter-quartile ranges (shading) of (a-f) north-facing and (g-l) south-facing wall (non-glass part) surface temperature differences (hourly) using $boi_{adj\leftarrow iso}$ and $boi_{adj\leftarrow a,5}$ or $boi_{adj\leftarrow a}$ in summer (JJA) and winter (DJF) in London for plan area fractions **(a,d,g,j)** λ_P=0.1, **(b,e,h,k)** λ_P=0.3, **(c,f,i,l)** λ_P=0.6.

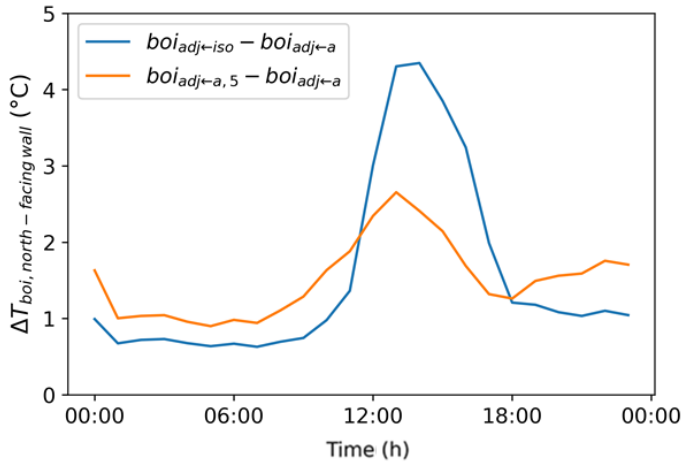

Fig. 9. London (λ_P = 0.6) clear winter day (30th December) diurnal differences in hourly north-facing wall surface temperature relative to $boi_{adj\leftarrow a}$ when using $boi_{adj\leftarrow iso}$ and $boi_{adj\leftarrow a,5}$.

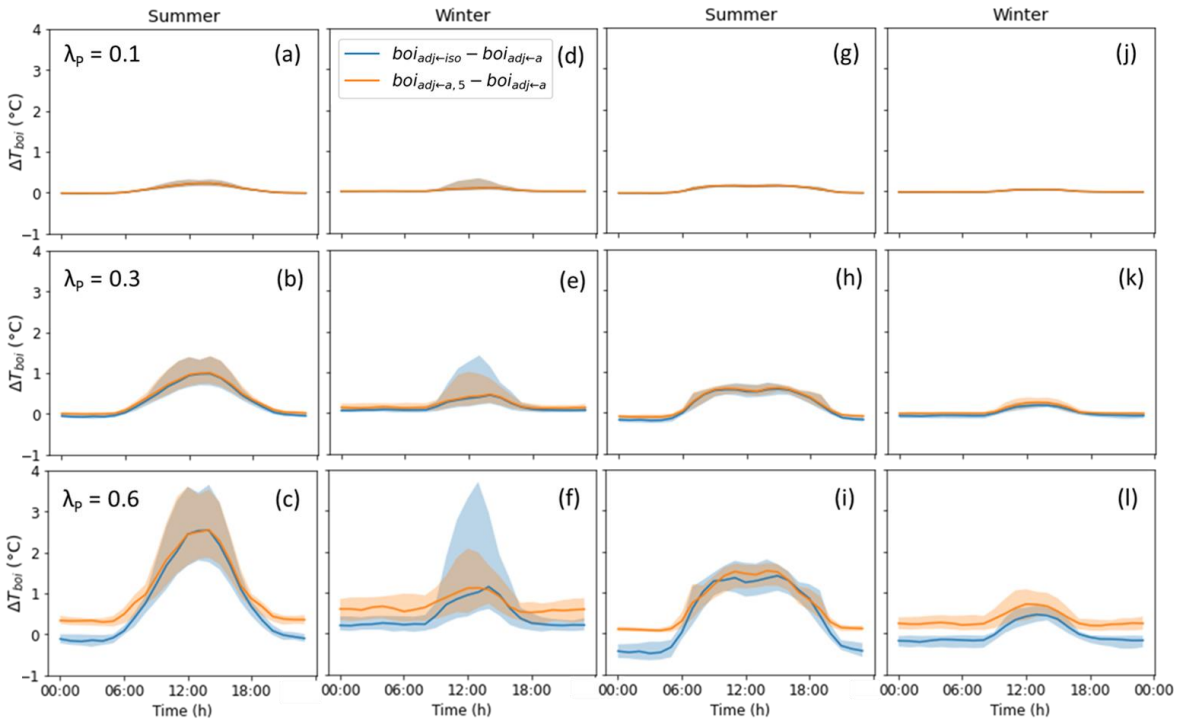

Fig. 10. As Fig. 8, but with $boi_{adj\leftarrow a}$ calculated with updated view factors.

3.4.Impact of longwave radiation method on building energy demand in London

Choice of longwave radiative exchange method (Table 1) impacts the annual cooling and heating energy demands. Simulations for London neighbourhoods with different λ_P show differences in energy demand, relative to base case ($boi_{adj\leftarrow a}$), to increase with λ_P (Table 3). The annual cooling energy demand is predicted to be larger using $boi_{adj\leftarrow iso}$ (cf. $boi_{adj\leftarrow a}$) by 12.4% (13% for $boi_{adj\leftarrow a,5}$), whereas annual heating energy demand is lower (cf. $boi_{adj\leftarrow a}$) by 3.1% (5% for $boi_{adj\leftarrow a,5}$) at λ_P = 0.6.

These differences are large compared to previous studies. For example, Evins et al.(2014) 's study in Geneva (unspecified λ_P) predicts a 5.1% increase in cooling energy and 3.5% decrease in heating energy ($boi_{adj\leftarrow a}$ to $boi_{adj\leftarrow iso}$). Similarly for Chicago (λ_P unknown), Luo et al. (2020) report a 0.2% - 3.2% increase in cooling energy and 0.2% - 3.6% decrease in heating energy (#1 to #3, Table 1). While Bouyer et al. (2011) model longwave radiation in an urban context (unspecified λ_P) in Lyon using a CFD-thermoradiative coupling with their own building energy model. They obtain a larger impact (19.1% increase in building cooling

energy and 9.3% decrease in heating energy) possibly due to the different simulation methods, building models and settings (e.g., building of interest - 7-stories located in a dense neighbourhood with large window-to-wall ratio - 66.7% glazing area on all facets). Also by using CFD, the local wind can be modified by the neighbourhood, which will further influence the surface temperatures and building energy consumption. While in our study the influence of neighbourhood on wind is not considered in this study, but is included in our new work (Tang et al., 2021).

This suggests neglecting neighbourhood characteristics' (λ_P) influence on inter-building longwave radiation simulations (Table 3) may result in important differences in energy demand predictions. The EnergyPlus default longwave radiative exchange method is suitable for buildings in areas with $\lambda_P < 0.1$ as the longwave radiation from *adj* buildings is relatively small, but not if simulating building thermal energy performance in a relatively denser urban area (e.g., $\lambda_P > 0.3$). The $boi_{adj \leftarrow iso}$ method tends to underpredict the annual cooling demand but overpredict the heating demand.

Diurnal cycles of cooling and heating loads difference are shown in Fig. 11. Consistent with the building external surface temperature pattern (Fig. 8, 9), the peak cooling load of $boi_{adj \leftarrow a}$ is the smallest and the heating load the highest. Similarly, peak load differences between the other two methods and the default method increase with λ_P. The heating load differences in the afternoon are closer to 0 at $\lambda_P = 0.1$ and 0.3 (Fig. 11b, d), because the more open neighbourhoods receive more solar radiation allowing the indoor air temperature to be above the heating setpoint (no heating is required). When $\lambda_P = 0.6$ (Fig. 11f), heating is needed during the whole day in winter in all cases, creating larger differences. In the densest neighbourhood ($\lambda_P = 0.6$), the peak cooling load difference between $boi_{adj \leftarrow a,5}$ and $boi_{adj \leftarrow a}$ could be as high as 4 W m^{-2} in summer (median), which is comparable to the internal heat

gain of 4.17 W m^{-2} used in these simulations. In winter, the median difference is larger than 1 W m^{-2}. Here, the nMBE (see section 2.4) is calculated with the hourly differences of cooling/heating load of $boi_{adj\leftarrow iso}$ and $boi_{adj\leftarrow a,5}$ (cf. $boi_{adj\leftarrow a}$). When λ_P = 0.6, hourly cooling load of both $boi_{adj\leftarrow iso}$ and $boi_{adj\leftarrow a,5}$ nMBE are around 12% in summer (not shown), and for winter heating load are -4% and -2%, respectively. The summer values clearly exceed the ASHRAE 10% uncertainty limits (section 2.4). Hence, using the EnergyPlus default longwave radiative exchange method could introduce a non-negligible bias into the simulated loads.

Table 3: (a) Annual cooling and heating energy demand and (b) percentage variation comparing with $boi_{adj\leftarrow a}$; (c) nMBE (section 2.4) of hourly load comparing with $boi_{adj\leftarrow a}$ in London for different λ_P.

		(a) Energy demand (kWh)			(b) Percentage variation (%)		(c) nMBE (%)	
	λ_P	$boi_{adj\leftarrow a}$	$boi_{adj\leftarrow a.5}$	$boi_{adj\leftarrow iso}$	$boi_{adj\leftarrow a.5}$	$boi_{adj\leftarrow iso}$	$boi_{adj\leftarrow a.5}$	$boi_{adj\leftarrow iso}$
Cooling	0.1	55.4	55.9	55.9	0.9	0.9	1.0	1.0
	0.3	46.0	47.8	47.7	3.8	3.6	4.0	3.9
	0.6	24.9	28.1	28.0	13.0	12.4	12.3	12.0
Heating	0.1	94.6	94.2	94.2	-0.5	-0.4	-0.3	-0.3
	0.3	96.9	95.0	95.3	-2.0	-1.6	-1.4	-1.2
	0.6	107.3	101.9	104.0	-5.0	-3.1	-3.7	-2.3

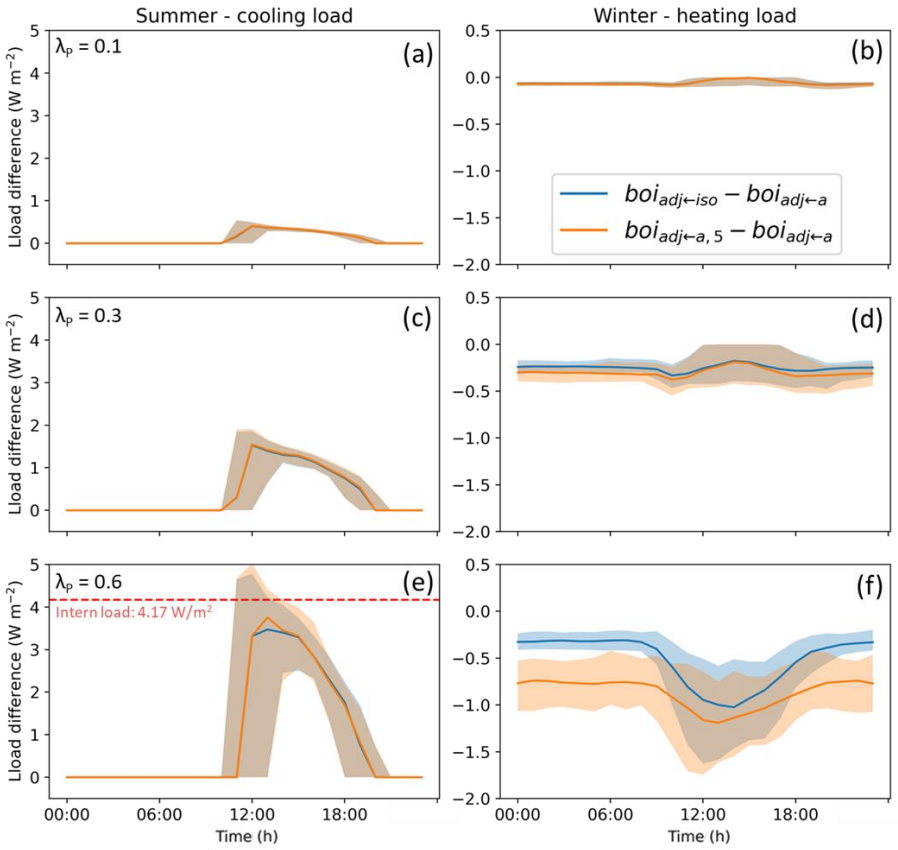

Fig. 11. Median diurnal cycle (lines) and inter-quartile range (shading) of hourly cooling load differences in

summer (JJA) and heating load differences in winter (DJF) from $boi_{adj \leftarrow a}$ (default method) in London for plan area fraction (**a,b**) λ_P=0.1, **(c,d)** λ_P=0.3, (**e,f**) λ_P=0.6. (**e**) internal load (red dashed line) provides a reference for comparison. **(b,d)** winter for λ_P = 0.1 and 0.3. All differences are < 0 because indoor temperatures are warmer than the setpoint, so heating system is not used.

3.5.Indoor overheating risk in London

To assess the impact on indoor overheating risk, we use the annual overheating degree hours above 26 °C and 28 °C (section 2.3) as the metric for our reference building in free-running condition in London (section 2.1). A building in a low-density neighbourhood (λ_P = 0.1) receives more shortwave radiation (than denser neighbourhoods) and therefore the overheating degree hours are larger (Table 4) given the other meteorological parameters (i.e., TMY weather data) are the same.

In the densest neighbourhood (λ_P = 0.6), the predicted overheating degree hours for $boi_{adj \leftarrow a,5}$ are higher during the both the day (18 %, time period defined in section 2.3) and night (43%, Table 4) when using the $boi_{adj \leftarrow a,5}$ (cf. $boi_{adj \leftarrow a}$). These biases are large and comparable to effects of increasing external wall insulation (Porritt et al. 2012). Porritt et al. (2012) identified increasing external wall insulation as one of most effective interventions for mitigating overheating, as it could reduce the degree hours for living rooms (> 28°C) by 20-22% and bedrooms (> 26 °C) by 49–51% in the UK climate. The $boi_{adj \leftarrow iso}$ method tends to underpredict the overheating risk (cf. $boi_{adj \leftarrow a,5}$), especially at night (12% less when λ_P = 0.6) as it cannot capture the effect of nocturnal longwave radiation trapping between buildings.

Another overheating criteria, maximum indoor operative temperature (T_{op}) (section 2.3), set by BS EN 15251 (BSI, 2007) and CIBSE TM52 (CIBSE, 2013), can be assessed based on diurnal cycles (Fig. 12). The median differences in T_{op} ($boi_{adj \leftarrow a,5}$ cf. $boi_{adj \leftarrow a}$) are 1.3 °C in summer. These are as large as the overheating risk assessment classes defined in BS EN 15251 (BSI, 2007) of 1 °C. Thus, the choice of longwave radiation method may lead to an overheating risk level misclassification. With night-time differences reaching 0.8 °C, and this

478 period of the day overheating will become more critical than daytime for free-running
479 buildings if occupants are indoors and unable to take adaptive interventions (e.g., open
480 windows) when sleeping (Anderson et al., 2013).

481 As the discrepancy between existing methods ($boi_{adj \leftarrow a}$ and $boi_{adj \leftarrow iso}$) is large, it is especially
482 critical to use the iterative/spin-up inter-building longwave calculating method when
483 assessing indoor overheating risk in cities.

484 **Table 4**: London with different λ_P. simulated (a) annual overheating degree hours and (b) percentage variation
485 (cf. $boi_{adj \leftarrow a}$, defined in section 2.4). Day (7:00 to 23:00, defined in section 2.3) and night (23:00 to 7:00) and
486 indoor operative temperature thresholds are 28 °C (day) and 26 °C (night) (CIBSE, 2006).

	λ_P	(a) Overheating degree hours			(b) Percentage variation (%)	
		$boi_{adj \leftarrow a}$	$boi_{adj \leftarrow a.5}$	$boi_{adj \leftarrow iso}$	$boi_{adj \leftarrow a.5}$	$boi_{adj \leftarrow iso}$
Day	0.1	16949	17147	17144	1.2	1.1
	0.3	14261	15045	14990	5.5	5.1
	0.6	7948	9398	9191	18.2	15.6
Night	0.1	602	619	619	2.8	2.8
	0.3	506	575	567	13.6	12.0
	0.6	314	450	411	43.3	31.0

487
488

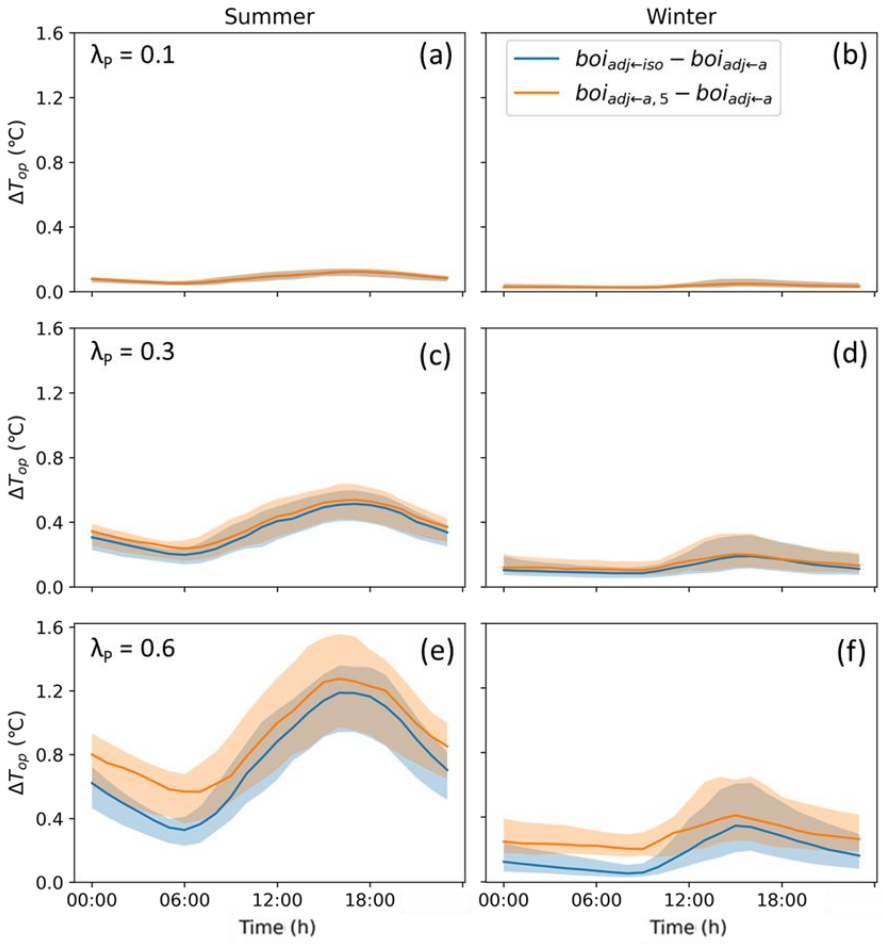

Fig. 12. As Fig. 11, but indoor operative temperature T_{op} differences.

3.6.Impact of latitude

To consider if these results vary with latitude and therefore solar altitude, we simulate a transect North (Aberdeen) and South (Marseille) of London. As the densest neighbourhood (λ_P = 0.6) has the largest differences, we only present the simulations for λ_P = 0.6.

3.6.1. North-facing wall surface temperature

As the north-facing wall surface temperature is most influenced by the increased inter-building longwave radiative exchange (section 3.3, Fig. 8), we select this for analysis. The surface temperature differences (Fig. 13) are generally larger for lower latitudes (i.e., Marseille > London > Aberdeen). The median midday simulated surface temperature using $boi_{adj\leftarrow a,5}$ are 2 °C warmer (cf. $boi_{adj\leftarrow a}$) in Aberdeen and 3 °C in Marseille in summer; whereas in winter these increases are slightly smaller (1.2 and 2.4 °C, respectively). The

nocturnal surface temperature differences are smaller between methods.

Thus, latitudinal variations in shortwave radiation impact the inter-building longwave exchange. As lower latitudes can have higher solar altitudes, the *adj* south-facing wall receives more solar radiation allowing higher surface temperature at noon. Therefore, the directly opposite *boi* north-facing wall receives more longwave radiation, increasing its surface temperature.

In winter, there is a large increase in midday surface temperatures for the $boi_{adj\leftarrow iso}$ method used for London and Marseille, as the shortwave radiation at lower latitudes increases the difference between south-facing wall surface temperature of the isolated building (used as T_{adj} of $boi_{adj\leftarrow iso}$) and air temperature (used as T_{adj} of $boi_{adj\leftarrow a}$) (Terjung and O'Rourke, 1981).

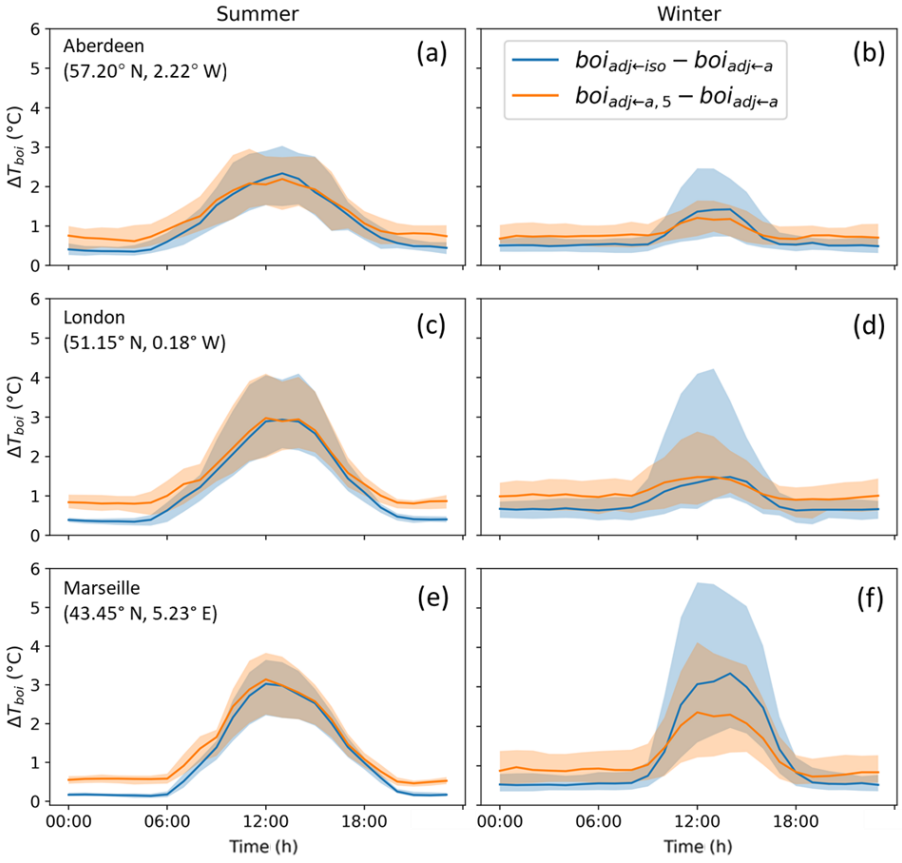

Fig. 13. As Fig. 8, but north-facing wall surface temperature differences (hourly) in three locations: (a,b) Aberdeen, (c,d) London, (e,f) Marseille for λ_P = 0.6.

3.6.2. Cooling/heating demand

As the latitude decreases, annual cooling energy demand difference between the $boi_{adj \leftarrow a,5}$ and $boi_{adj \leftarrow a}$ methods decreases (17% to 9%, Table 5) while difference in heating demand increases (4% to 6%). Whereas, the trend in absolute difference in energy demand is the opposite (Table 5: annual cooling demand increases from 1.7 (Aberdeen) to 5.8 kWh (Marseille) and heating decreases (5.2 to 3.7 kWh). Relative differences in energy demand are commonly compared (e.g. Evins et al., 2014; Luo et al., 2020), but as absolute consumption impacts both cost and carbon emission, it should not be neglected.

Diurnal median peak cooling load differences between methods ($boi_{adj \leftarrow a,5}$ and $boi_{adj \leftarrow a}$) occur in around the mid-day and increase with decreasing latitude from 3 to 4.5 W m^{-2} (Fig. 14) and the equivalent peak heating load differences are also larger (0.8 to 1.2 W m^{-2}) and appearing during the similar period (except Marseille). In Marseille, a fluctuation near mid-day impacts the heating when the indoor air temperature exceeds the heating setpoint (no heating is required). These trends of differences are consistent with diurnal cycle of cooling and heating loads, and hence are potentially influences by building-related settings. For instance, lowering the cooling setpoint and raising the heating setpoint can expand the period of HVAC system operation and may potentially increase the absolute differences in energy demand. Orientation of windows affect the time period when the indoor space is exposed to direct sunlight as well as the intensity, therefore influences the cooling/heating loads (Raftery et al., 2014). Other building envelope features (e.g. insulation, thermal mass and wind-to-wall ratios) will have an impact but are beyond the scope of this study.

As shown in Table 5, summer hourly cooling load nMBE for $boi_{adj \leftarrow a.5}$ and $boi_{adj \leftarrow iso}$ (cf. $boi_{adj \leftarrow a}$) in both Aberdeen and London are exceeding the ASHRAE ±10% uncertainty limit (section 2.4). This demonstrates the bias of simulated cooling (heating) load with EnergyPlus default longwave radiative exchange method is larger for higher (lower) latitudes.

Table 5: As Table 3, but for locations at three latitudes. Percentage variation is related to the base value (cf. $boi_{adj\leftarrow a}$).

		(a) Energy Demand (kWh)			(b) Percentage variation (%)		(c) nMBE (%)	
	λ_P = 0.6	$boi_{adj\leftarrow a}$	$boi_{adj\leftarrow a.5}$	$boi_{adj\leftarrow iso}$	$boi_{adj\leftarrow a.5}$	$boi_{adj\leftarrow iso}$	$boi_{adj\leftarrow a.5}$	$boi_{adj\leftarrow iso}$
Cooling	Aberdeen	10.0	11.7	11.7	17.1	17.3	15.3	15.4
	London	24.9	28.1	28.0	13.0	12.4	12.3	12.0
	Marseille	61.2	67.0	66.6	9.4	8.8	8.3	7.8
Heating	Aberdeen	129.2	124.0	125.7	-4.1	-2.7	-2.7	-1.7
	London	107.3	101.9	104.0	-5.0	-3.1	-3.7	-2.3
	Marseille	59.8	56.1	57.6	-6.2	-3.7	-5.4	-3.5

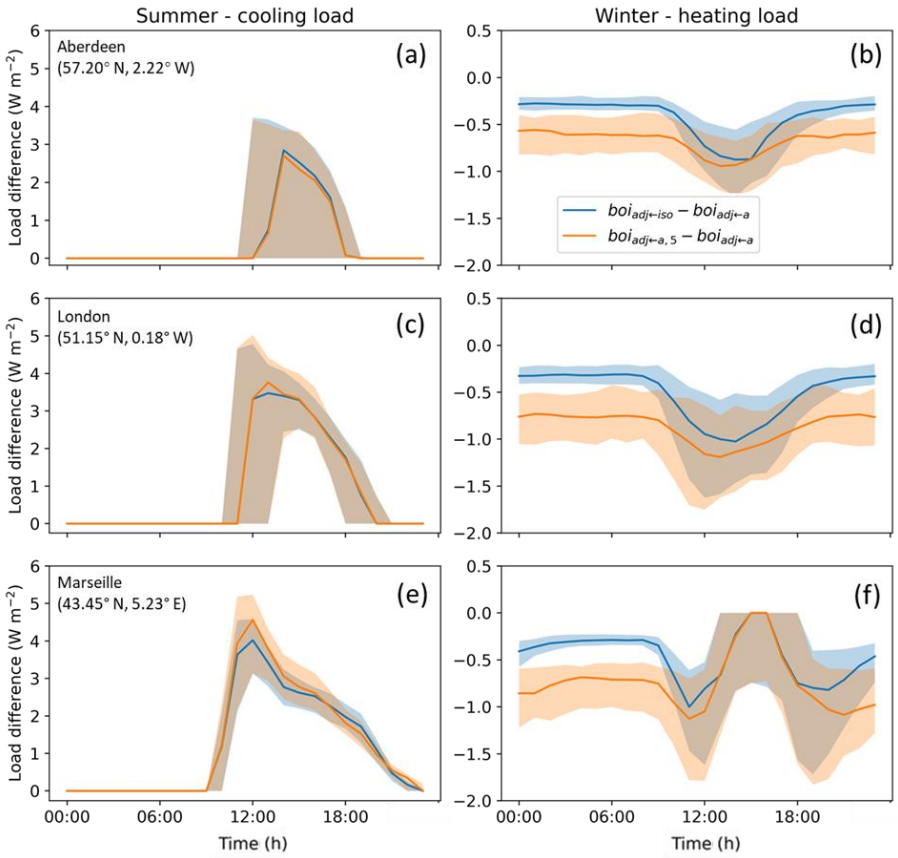

Fig. 14. As Fig. 13 but cooling/heating load differences. In winter, Marseille's differences are all less than 0 because of indoor temperatures being warmer than the setpoint, so heating system is not used.

3.6.3. Overheating risk

The annual overheating degree hours (Table 6), have a similar trend to the cooling energy demand (Table 5) with larger relative differences in Aberdeen because of the lower base value (60% at night, cf. 43% in London, 20 % in Marseille). The absolute difference in overheating degree hours is the largest in Marseille (Table 6). Diurnal median operative temperature differences (Fig. 15) indicate the default method tends to underestimate the peak,

555 especially at lower latitudes. Summer median difference in peak increase from 1 °C in
556 Aberdeen to 1.35 °C in Marseille (Fig. 15). As a bias of 1 °C can cause overheating risk
557 misclassification (section 3.4), even in Aberdeen the default method underestimation should
558 not be ignored.

559 **Table 6**: As Table 4, but for three locations. Percentage variation is related to the base value (cf. $boi_{adj\leftarrow a}$).

		(a) Overheating degree hours			(b) Percentage variation (%)	
		$boi_{adj\leftarrow a}$	$boi_{adj\leftarrow a.5}$	$boi_{adj\leftarrow iso}$	$boi_{adj\leftarrow a.5}$	$boi_{adj\leftarrow iso}$
Day	Aberdeen	2491	3102	3050	24.5	22.4
	London	7948	9398	9191	18.2	15.6
	Marseille	22258	25093	24666	12.7	10.8
Night	Aberdeen	39	62	619	60.1	46.5
	London	314	450	411	43.3	31.0
	Marseille	2814	3387	3216	20.4	14.3

560
561

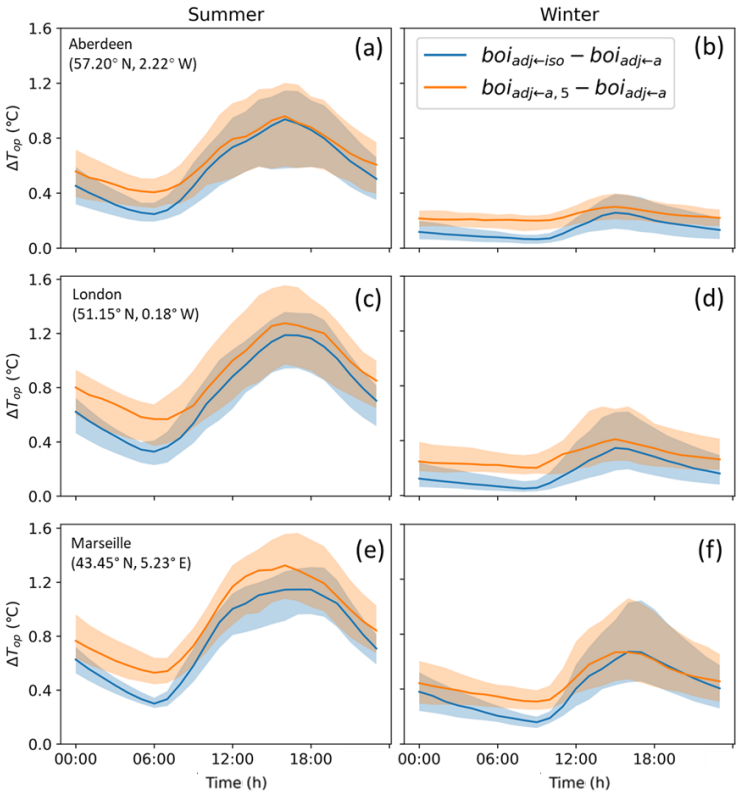

562
563 **Fig. 15.** As Fig 12, but indoor operative temperature differences (hourly) in three locations: (**a,b**) Aberdeen,
564 (**c,d**) London, (**e,f**) Marseille for λ_P = 0.6.
565

566 ## 4. Discussion

567 Prior work documented the importance of considering external longwave radiation in
568 building energy simulations (Bouyer et al., 2011; Evins et al., 2014; Luo et al., 2020), but did
569 not assess plan area ratios of different neighbourhoods. We apply an iterative/spin-up

approach to the widely-used building energy simulation tool (i.e., EnergyPlus) to better determine the impacts of longwave radiative exchanges between buildings and further improve usability of the tool. One advantage of our proposed approach is that it does not require extra external data inputs apart from the supply of view factors, which can be calculated in a variety of ways (e.g., Howell et al., 2010). Thus, the approach can be easily and widely applied to assess the impact of the urban setting on building internal and external thermal conditions and energy performance.

Our findings extend current understanding of external longwave radiation on buildings by considering changes in urban plan area density and latitude. As denser neighbourhoods have larger building view factors, rather than sky, the longwave radiative fluxes between buildings are greater. Solar altitudes are larger for lower latitudes, which causes less shading on external building surfaces and higher surface temperatures, hence emitting greater longwave radiation. Therefore, differences in all metrics (e.g. energy demand and indoor overheating risk) compared to the default EnergyPlus option are found to be more evident in denser neighbourhoods. This indicates that the benefits gained from the updated approach may be particularly important for buildings located in dense neighbourhoods and low latitudes. As the urban population growth is expected to be greater at lower latitudes (United Nations, 2019) with increasing neighbourhood densities, our approach has a large potential to ensure more sustainable designs in these regions if taken into account.

However, in our present work we use idealised neighbourhoods with identical buildings. In many neighbourhoods that may be reasonable but where there is a heterogenous mix of buildings, the surface temperature of adjacent buildings could be calculated by treating them as isolated individuals (Luo et al., 2020), as we find this bias to be smaller than the EnergyPlus default option. However, further improvement is needed for dense heterogenous

neighbourhoods in low latitudes. Currently, the ground surface temperature is not updated (i.e. remains the same as air temperature from TMY inputs), this should be further explored in the future. Furthermore, we only consider one building type, many design options will have an impact (e.g. envelope features, building heights) on the outdoor variables and feedback to the indoor thermal environment in various ways, therefore could also be explored in future research.

5. Conclusions

Using EnergyPlus, the surface temperature for an adjacent building can be simulated using the air temperature provided (e.g. TMY) or from an isolated building if simulating inter-building longwave radiative exchange. If these air temperature data are observations are based on standard WMO rural climate settings, they will not represent the urban climate properly (Tang et al., 2021; WMO, 2018). We conclude that none of the existing EnergyPlus methods allow realistic simulations if the building of interest (*boi*) is within a neighbourhood surrounded by other buildings. Here, we propose a model spin-up approach to account for adjacent buildings surface temperatures. When compared to existing methods to determine inter-building longwave radiative exchange, the surface temperature, building energy demand and overheating risks in various plan area fractions and climates are impacted. Key conclusions are:

- At least five iterations/spin-up are needed when simulating the inter-building longwave radiative exchange in EnergyPlus, especially in dense neighbourhoods (λ_P = 0.6). With sufficient iterations, the initial adjacent building surface temperature chosen no longer matters.
- Comparing the default EnergyPlus longwave radiative exchange method (assigning air temperature to adjacent building surfaces) to the spin-up method we propose:
    - Differences in metrics are small for low density neighbourhoods (λ_P = 0.1) but

increase to unignorable for denser neighbourhoods (λ_P = 0.3 and 0.6).

- Median external building surface temperature is underpredicted by up to 3 °C, which could become even larger with lower latitudes.
- Annual cooling energy demand is underpredicted (up to 17%) and heating energy demand overpredicted (up to 6%) varying with climates when λ_P = 0.6. For lower latitudes, the absolute difference in peak cooling and heating loads are larger.
- Annual overheating degree hours are underpredicted in the day (up to 25%) and night (60%) (λ_P = 0.6). Lower latitudes have larger absolute differences, but the relative differences tend to decrease. The median indoor operative temperature is underestimated, with larger impacts at lower latitudes (up to 1.4 °C).

- Using isolated building surface temperatures for adjacent buildings in a neighbourhood, nocturnal wall surface temperature is underpredicted (up to 0.6 °C). The winter north-facing wall temperature is largely overpredicted (~2 °C). Annual cooling demand is underpredicted (up to 0.6%) and heating overpredicted (up to 2.5%). Overall, indoor overheating risk is underpredicted, especially at night (up to 13.6%).

6. Acknowledgement

This work is funded as part of NERC-COSMA project (NE/S005889/1) and Newton Fund/Met Office CSSP China Next Generation Cities (SG, ZL).

7. References

Allegrini, J., Dorer, V., Carmeliet, J., 2012. Influence of the urban microclimate in street canyons on the energy demand for space cooling and heating of buildings. Energy Build. 55, 823–832.

Allegrini, J., Dorer, V., Carmeliet, J., 2016. Impact of radiation exchange between buildings in urban street canyons on space cooling demands of buildings. Energy Build. 127, 1074–1084.

Anderson, M., Carmichael, C., Murray, V., Dengel, A., Swainson, M., 2013. Defining indoor heat thresholds for health in the UK. Perspect. Public Health 133, 158–164.

ANSI/ASHRAE, 2011. Standard Method of Test for the Evaluation of Building Energy Analysis Computer Programs. Atlanta.

Arasteh, D., Kohler, C., Griffith, B., 2009. Modeling Windows in Energy Plus with Simple Performance Indices. Berkeley.
ASHRAE, 2001. International Weather for Energy Calculations (IWEC Weather Files) Users Manual and CD-ROM. ASHRAE, Atlanta.
ASHRAE, 2014. ASHRAE Guideline 14: Measurement of Energy, Demand, and Water Savings. Atlanta.
Best, M.J., Grimmond, C.S.B., 2014. Importance of initial state and atmospheric conditions for urban land surface models' performance. Urban Clim. 10, 387–406.
Boccalatte, A., Fossa, M., Gaillard, L., Menezo, C., 2020. Microclimate and urban morphology effects on building energy demand in different European cities. Energy Build. 224, 110129.
Bouyer, J., Inard, C., Musy, M., 2011. Microclimatic coupling as a solution to improve building energy simulation in an urban context. Energy Build. 43, 1549–1559.
BSI, 2007. BS EN 15251: 2007: Indoor environmental parameters for design and assessment of energy performance of buildings- addressing indoor air quality, thermal environment, lighting and acoustics. British Standards Institution, London.
Bueno, B., Norford, L., Pigeon, G., Britter, R., 2011. Combining a Detailed Building Energy Model with a Physically-Based Urban Canopy Model. Boundary-Layer Meteorol. 140, 471–489.
Chan, A.L.S., 2011. Developing a modified typical meteorological year weather file for Hong Kong taking into account the urban heat island effect. Build. Environ. 46, 2434–2441.
Ciancio, V., Falasca, S., Golasi, I., Curci, G., Coppi, M., Salata, F., 2018. Influence of Input Climatic Data on Simulations of Annual Energy Needs of a Building: EnergyPlus and WRF Modeling for a Case Study in Rome (Italy). Energies 11, 2835.
CIBSE, 2006. CIBSE Guide A: Environmental design, 7th ed. Chartered Institution of Building Services Engineers, London.
CIBSE, 2013. TM52: The Limits of Thermal Comfort: Avoiding Overheating in European Buildings. Chartered Institution of Building Services Engineers, London.
Demanuele, C., Mavrogianni, A., Davies, M., Kolokotroni, M., Rajapaksha, I., 2012. Using localised weather files to assess overheating in naturally ventilated offices within London's urban heat island. Build. Serv. Eng. Res. Technol. 33, 351–369.
Evins, R., Dorer, V., Carmeliet, J., 2014. Simulating external longwave radiation exchange for buildings. Energy Build. 75, 472–482.
Gracik, S., Heidarinejad, M., Liu, J., Srebric, J., 2015. Effect of urban neighborhoods on the performance of building cooling systems. Build. Environ. 90, 15–29.
Grimmond, C.S.B., Oke, T.R., 1999. Aerodynamic Properties of Urban Areas Derived from Analysis of Surface Form. J. Appl. Meteorol. 38, 1262–1292.
Han, Y., Taylor, J.E., Pisello, A.L., 2017. Exploring mutual shading and mutual reflection inter-building effects on building energy performance. Appl. Energy 185, 1556–1564.
Howell, J.R., Siegel, R., Menguc, M.P., 2010. Thermal radiation heat transfer, 5th ed. CRC Press LLC, Bosa Roca.
Hwang, R.-L., Lin, C.-Y., Huang, K.-T., 2017. Spatial and temporal analysis of urban heat island and global warming on residential thermal comfort and cooling energy in Taiwan. Energy Build. 152, 804–812.
Kanda, M., Kanega, M., Kawai, T., Moriwaki, R., Sugawara, H., 2007. Roughness Lengths for Momentum and Heat Derived from Outdoor Urban Scale Models. J. Appl. Meteorol. Climatol. 46, 1067–1079.
Kesten, D., Tereci, A., Strzalka, A.M., Eicker, U., 2012. A method to quantify the energy performance in urban quarters. In: HVAC and R Research. pp. 100–111.
Lima, I., Scalco, V., Lamberts, R., 2019. Estimating the impact of urban densification on

698 high-rise office building cooling loads in a hot and humid climate. Energy Build. 182,
699 30–44.
700 Liu, J., Heidarinejad, M., Gracik, S., Srebric, J., 2015. The impact of exterior surface
701 convective heat transfer coefficients on the building energy consumption in urban
702 neighborhoods with different plan area densities. Energy Build. 86, 449–463.
703 Luo, X., Hong, T., Tang, Y.-H., 2020. Modeling Thermal Interactions between Buildings in
704 an Urban Context. Energies 13, 2382.
705 Martinopoulos, G., Serasidou, A., Antoniadou, P., Papadopoulos, A.M., 2018. Building
706 Integrated Shading and Building Applied Photovoltaic System Assessment in the Energy
707 Performance and Thermal Comfort of Office Buildings. Sustainability 10, 4670.
708 Mavrogianni, A., Wilkinson, P., Davies, M., Biddulph, P., Oikonomou, E., 2012. Building
709 characteristics as determinants of propensity to high indoor summer temperatures in
710 London dwellings. Build. Environ. 55, 117–130.
711 Miller, C., Thomas, D., Kämpf, J., Schlueter, A., 2018. Urban and building multiscale co-
712 simulation: case study implementations on two university campuses. J. Build. Perform.
713 Simul. 11, 309–321.
714 Morrison, W., Kotthaus, S., Grimmond, C.S.B., Inagaki, A., Yin, T., Gastellu-Etchegorry,
715 J.P., Kanda, M., Merchant, C.J., 2018. A novel method to obtain three-dimensional
716 urban surface temperature from ground-based thermography. Remote Sens. Environ.
717 215, 268–283.
718 Morrison, W., Kotthaus, S., Grimmond, S., 2021. Urban surface temperature observations
719 from ground-based thermography: intra- and inter-facet variability. Urban Clim. 35,
720 100748.
721 Morrison, W., Yin, T., Lauret, N., Guilleux, J., Kotthaus, S., Gastellu-Etchegorry, J.-P.P.,
722 Norford, L., Grimmond, S., 2020. Atmospheric and emissivity corrections for ground-
723 based thermography using 3D radiative transfer modelling. Remote Sens. Environ. 237,
724 111524.
725 Oikonomou, E., Davies, M., Mavrogianni, A., Biddulph, P., Wilkinson, P., Kolokotroni, M.,
726 2012. Modelling the relative importance of the urban heat island and the thermal quality
727 of dwellings for overheating in London. Build. Environ. 57, 223–238.
728 Oke, T.R., 1982. The energetic basis of the urban heat island. Q. J. R. Meteorol. Soc. 108, 1–
729 24.
730 Oleson, K.W., Bonan, G.B., Feddema, J., Jackson, T., 2011. An examination of urban heat
731 island characteristics in a global climate model. Int. J. Climatol. 31, 1848–1865.
732 Porritt, S., Shao, L., Cropper, P., Goodier, C., 2011. Adapting dwellings for heat waves.
733 Sustain. Cities Soc. De Montfort University.
734 Porritt, S.M.M., Cropper, P.C.C., Shao, L., Goodier, C.I.I., 2012. Ranking of interventions to
735 reduce dwelling overheating during heat waves. Energy Build. 55, 16–27.
736 Raftery, P., Lee, E., Webster, T., Hoyt, T., Bauman, F., 2014. Effects of furniture and
737 contents on peak cooling load. Energy Build. 85, 445–457.
738 Ramponi, R., Gaetani, I., Angelotti, A., 2014. Influence of the urban environment on the
739 effectiveness of natural night-ventilation of an office building. Energy Build. 78, 25–34.
740 Ruiz, G.R., Bandera, C.F., 2017. Validation of calibrated energy models: Common errors.
741 Energies 10, 1587.
742 Salvati, A., Coch Roura, H., Cecere, C., 2017. Assessing the urban heat island and its energy
743 impact on residential buildings in Mediterranean climate: Barcelona case study. Energy
744 Build. 146, 38–54.
745 Santamouris, M., Papanikolaou, N., Livada, I., Koronakis, I., Georgakis, C., Argiriou, A.,
746 Assimakopoulos, D.., 2001. On the impact of urban climate on the energy consumption
747 of buildings. Sol. Energy 70, 201–216.

Tang, Y., Sun, T., Luo, Z., Omidvar, H., Theeuwes, N., Xie, X., Xiong, J., Yao, R., Grimmond, S., 2021. Urban meteorological forcing data for building energy simulations. Build. Environ. 204, 108088.
Terjung, W.H., O'Rourke, P.A., 1981. Energy input and resultant surface temperatures for individual urban interfaces, selected latitudes and seasons. Arch. Meteorol. Geophys. Bioclimatol. Ser. B 29, 1–22.
U.S. Department of Energy, 2020a. Chapter 1: Overview. In: EnergyPlus Version 9.4.0 Documentation: Engineering Reference. pp. 20–24.
U.S. Department of Energy, 2020b. Chapter 3: Surface Heat Balance Manager / Processes. In: EnergyPlus Version 9.4.0 Documentation: Engineering Reference. pp. 58–168.
U.S. Department of Energy, 2020c. Chapter 5: Climate, Sky and Solar/Shading Calculations. In: EnergyPlus Version 9.4.0 Documentation: Engineering Reference. pp. 187–224.
U.S. Department of Energy, 2020d. Chapter 17: Simulation Models – Encyclopedic Reference. In: EnergyPlus Version 9.4.0 Documentation: Engineering Reference. pp. 1277–1325.
United Nations, 2019. World Population Prospects 2019: Highlights. New York.
Vallati, A., Mauri, L., Colucci, C., 2018. Impact of shortwave multiple reflections in an urban street canyon on building thermal energy demands. Energy Build. 174, 77–84.
Vartholomaios, A., 2017. A parametric sensitivity analysis of the influence of urban form on domestic energy consumption for heating and cooling in a Mediterranean city. Sustain. Cities Soc. 28, 135–145.
Virk, G., Mylona, A., Mavrogianni, A., Davies, M., 2015. Using the new CIBSE design summer years to assess overheating in London: Effect of the urban heat island on design. Build. Serv. Eng. Res. Technol. 36, 115–128.
Winkelmann, F.C., 2001. Modeling Windows in EnergyPlus. Proc. Build. Simul. 2001 1–11.
WMO, 2018. Guide to meteorological instruments and methods of observation, 2018th ed. WMO, Geneva.
Yang, X., Yao, L., Peng, L.L.H., Jiang, Z., Jin, T., Zhao, L., 2019. Evaluation of a diagnostic equation for the daily maximum urban heat island intensity and its application to building energy simulations. Energy Build. 193, 160–173.
Yang, X., Zhao, L., Bruse, M., Meng, Q., 2012. An integrated simulation method for building energy performance assessment in urban environments. Energy Build. 54, 243–251.
Zhang, R., Lam, K.P., Yao, S., Zhang, Y., 2013. Coupled EnergyPlus and computational fluid dynamics simulation for natural ventilation. Build. Environ. 68, 100–113.
Zhang, Y., Lin, K., Zhang, Q., Di, H., 2006. Ideal thermophysical properties for free-cooling (or heating) buildings with constant thermal physical property material. Energy Build. 38, 1164–1170.

Supplementary Material

SM.1. Assessment of view factors calculated with Monte Carlo ray-tracing method

The fundamental expression of view factors between two finite surfaces ($F_{1\to2}$) is (Howell et al., 2010):

$$F_{1\to2} = \frac{1}{A_1}\int_{A_1}\int_{A_2}\frac{\cos\theta_1\cos\theta_2}{\pi r_{12}^2}dA_2dA_1 \qquad \text{(S.1)}$$

where surfaces 1 and 2 have areas of A_1 and A_2 (m^2) and have their normal at angle θ_1 and θ_2 (rad) to the line of length r_{12} (m) between them.

The view factor between the *boi* north-facing wall and *adj* south-facing wall in the neighbourhood with λ_P = 0.1 (Fig. S.1) calculated with the Monte Carlo ray-tracing method (Eq. 10) are compared to the result calculated with Eq. S.1. With 3000 rays the view factor difference between the Monte Carlo ray-tracing result and Eq. S.1 is < 1 x 10^{-5} (Fig. S.2).

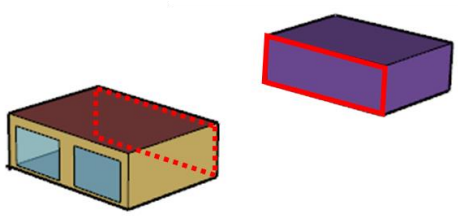

Fig. S.1. Two surfaces selected for view factor calculation indicated by red boxes.

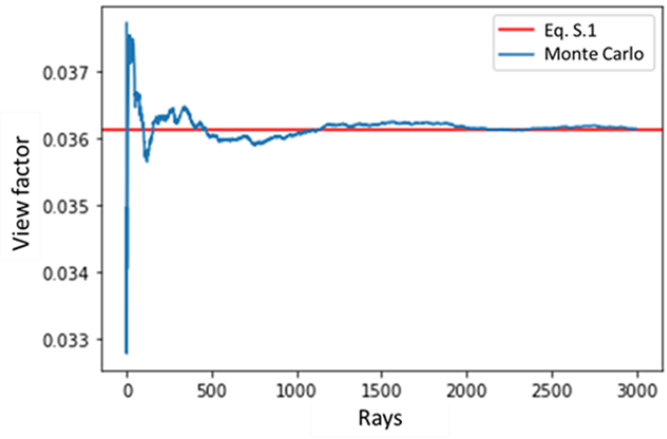

Fig. S.2. View factors calculated with Monte Carlo method and Eq. S.1.

SM.2. Impact of simplification of adjacent building modelling

Adjacent building facets are assumed to be isotropic during the simulation to save computational cost. The impact of this simplification has been analysed by comparing the simplified detailed facet modelling of the case $boi_{adj \leftarrow a,5}$ with λ_P = 0.6. The north-facing wall (which directly faces windows on adjacent buildings) surface temperature differences are shown in Fig. S.5. The median difference in north-facing wall surface temperature due to

809 windows simplification is up to 0.2 °C. For other walls, this difference is much smaller (not
810 shown) as they are not facing windows directly.

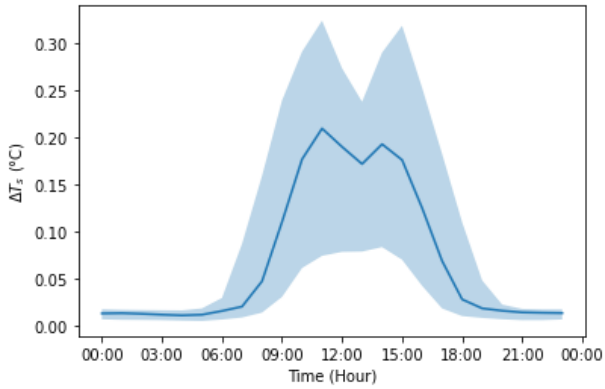

811
812 **Fig. S.3**. Median diurnal cycle (lines) and inter-quartile ranges (shading) of north-facing wall surface
813 temperature differences (hourly) using $boi_{adj\leftarrow a,5}$ (simplified model – detailed model) during the year in London
814 for plan area fractions λ_P=0.6.

815 SM.3. Differences of external building surface temperatures between iterations – extended

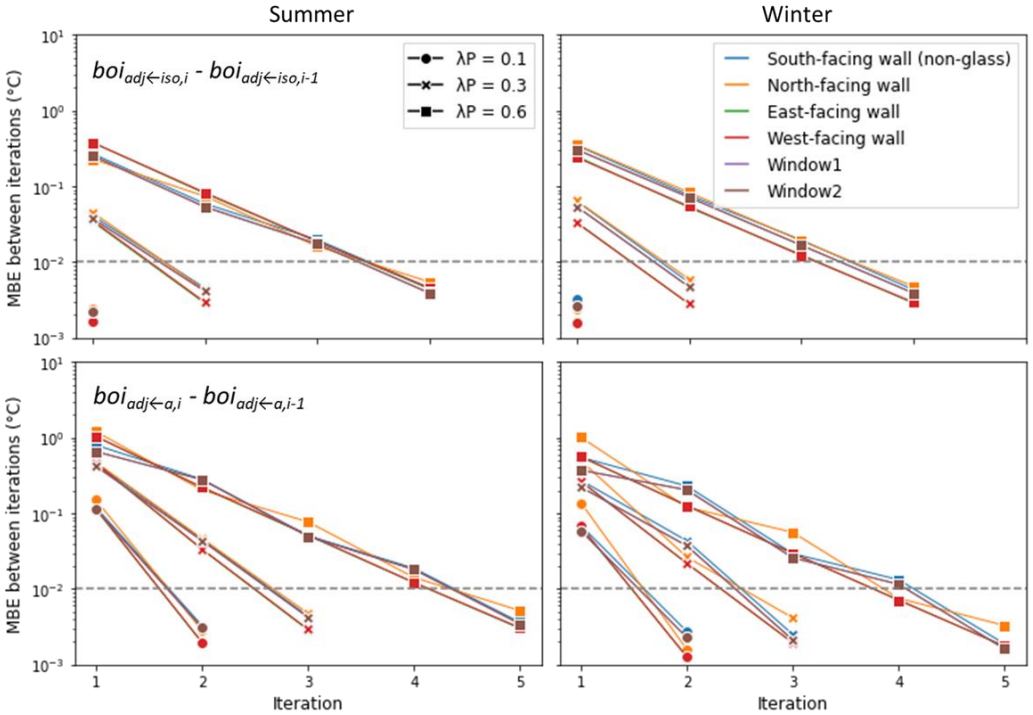

816
817 **Fig. S.4.** Summer (JJA) and winter (DJF) mean bias error (MBE, section 2.4; 10-min timestep, *N*=52560) in
818 external building surface temperature (cf. previous iteration, Fig. 2) for different facets (colour) in London with
819 three plan area fractions (λ_P) (marker) and two initial *adj* surface temperatures (rows) with the convergence
820 criteria (0.01 °C, dashed line). Annual MBE are shown in Figure 4.

821

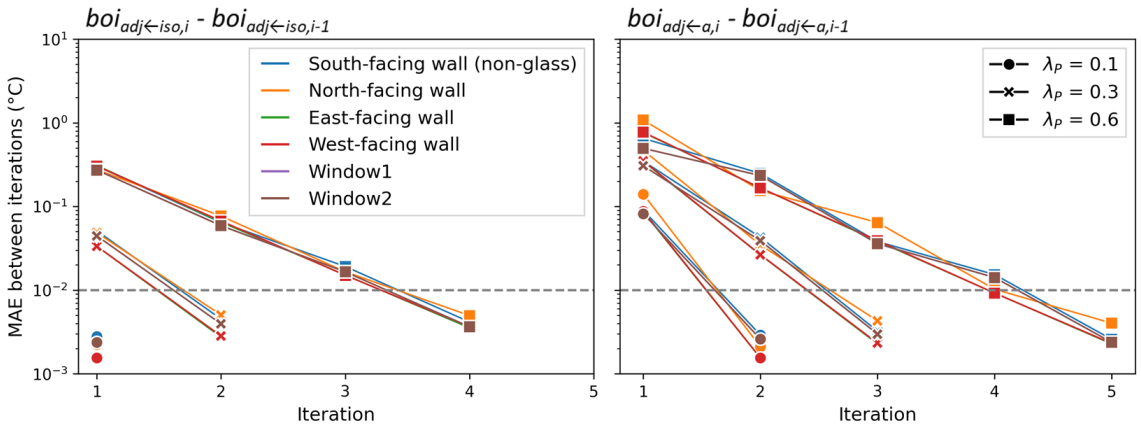

Fig. S.5. Annual mean absolute error (MAE, section 2.4; 10-min timestep, *N*=52560) in external building surface temperature (cf. previous iteration, Fig. 2) for different facets (colour) in London with three plan area fractions (λ_P) (marker) and two initial *adj* surface temperatures (rows) with the convergence criteria (0.01 °C, dashed line). MBE are shown in Figure 4.

SM.4. Differences between surface temperatures simulated with different sources of initial surface temperature values at each iteration– extended

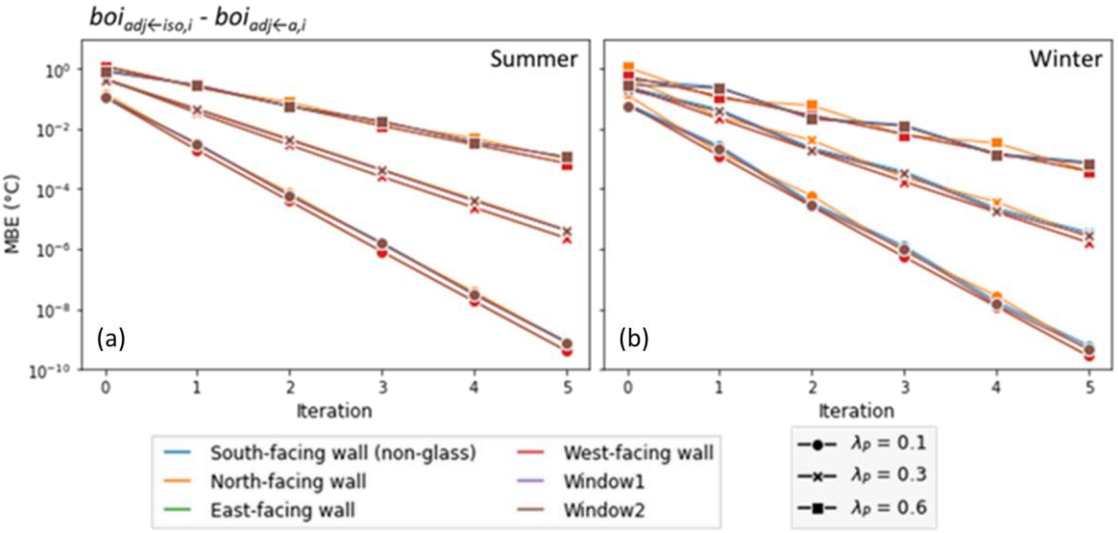

Fig. S.6. Impact of different initialisations (Fig 2; i.e. iteration 0 refers to $boi_{adj\leftarrow iso}$ - $boi_{adj\leftarrow a}$) on external building surface temperature (metric MBE between results, section 2.4; 10-min timestep, *N*=52560) for different facets (colour) in London with three plan area fractions (λ_P, marker) for (a) summer (JJA) and (b) winter (DJF). Annual MBE are shown in Figure 6.

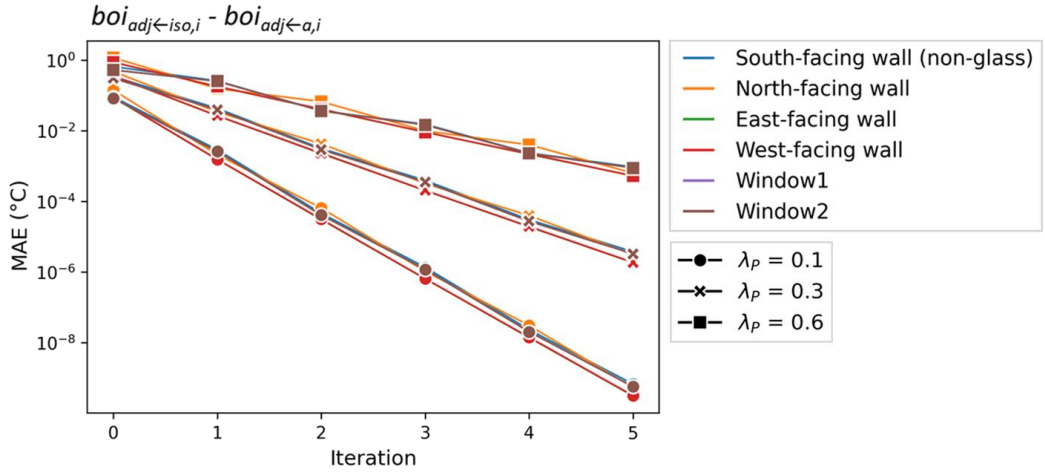

Fig. S.7. Annual mean absolute error (MAE, section 2.4; 10-min timestep, N=52560) in external building surface temperature between iterated results with different initialisations (Fig 2; i.e. iteration 0 refers to $boi_{adj\leftarrow iso}$ - $boi_{adj\leftarrow a}$) for different facets (colour) in London with three plan area fractions (λ_P, marker). Annual MBE are shown in Figure 6.